eprints@whiterose.ac.uk
https://eprints.whiterose.ac.uk/

Role of soluble aluminum species in the activating solution for synthesis of silico-aluminophosphate geopolymers

Yan-Shuai Wang[1], John L. Provis[2*] and Jian-Guo Dai[3*]

[1] PhD Candidate, Department of Civil and Environmental Engineering, The Hong Kong Polytechnic University, Hong Kong, China

[2] Professor, Department of Materials Science and Engineering, University of Sheffield, Sir Robert Hadfield Building, Portobello Street, Sheffield, UK. Corresponding author: j.provis@sheffield.au.uk

[3] Professor, Department of Civil and Environmental Engineering, The Hong Kong Polytechnic University, Hong Kong, China. Corresponding author: cejgdai@polyu.edu.hk

1 **Abstract:**

2

3   An aluminosilicate precursor, such as metakaolin, can be transformed into a cement-like

4 geopolymer binder via a phosphate activation approach. This paper identifies the effect of the

5 addition of aluminum species into the phosphate activating solution on the formation of such

6 geopolymers, from the fresh to the hardened state. Activating solutions with Al/P molar ratios

7 of 0, 0.1, and 0.3 were prepared by blending monoaluminum phosphate (MAP) and

8 orthophosphoric acid (OPA). The rheological properties, fluidity, and setting times of the fresh

9 geopolymer pastes and the compressive strength of the hardened geopolymer matrices were

10 studied. Liquid-state ^{27}Al and ^{31}P nuclear magnetic resonance (NMR) measurements for the

11 chemical environments of Al and P, and spectroscopic, thermal, and microscopic analyses

12 revealed that the soluble aluminum in the phosphate activating solution played an important

13 role during the geopolymerization process. Seeding of aluminum species through inclusion in

14 the activating solution allowed a rapid sol/gel transition that improved the rheological

15 properties and setting time of the fresh geopolymer pastes at ambient temperature. However,

16 although the increased concentration of aluminum phosphate oligomers promoted by the

17 soluble aluminum addition contributed to the formation of a compact matrix with high early

18 strength, it hinders the ongoing reaction of metakaolin in the later period, which has a

19 detrimental influence on ongoing strength development beyond 7 days of curing.

20

25

26

27

28

29

30

31

32

33

34

1. Introduction

The term "geopolymer" is often used to describe an inorganic polymeric material with polymer-like poly-aluminosilicate chains or networks [1]. Its formation is based on the reaction between an aluminosilicate precursor and an activating solution, which promotes the dissolution of the particulate precursor, and the consequent polycondensation of high-connectivity silicate networks as binding phases to form a hardened material [2, 3]. Compared to Portland cement, the geopolymer material is becoming a strong competitor due to its attractive features of sustainability and durability [4], especially when life cycle assessment (LCA)-based mix design technology of geopolymers is effectively applied [5]. Besides, geopolymer-made products can exhibit excellent thermal stability or fire-resistance [1], mechanical performance [6] and chemical anticorrosion properties (e.g., against acid, sulfate and chloride attack) [7].

The formation of geopolymer binders is conventionally based on alkali activation of aluminosilicates, where the hydroxide ions enable the dissolution of the solid aluminosilicate precursors to form isolated aluminate and silicate anions, and the elevated concentrations of these species in the aqueous state then drive polymerization, also involving hydrated cations to charge-balance, by reforming the aluminosilicate bonds [8]. However, an alternative activation approach for the aluminosilicate sources is phosphate activation [9, 10], which involves an analogous acid-activated reaction process involving phosphoric acid. The mechanism of phosphate-activated geopolymerization starts with the dealumination of the aluminosilicate source (i.e., dealumination reaction) into the acidic aqueous environment, following the polycondensation of free aluminate, silicate, and phosphate units to generate Si-O-Al, Si-O-P and/or Al-O-P bonds in silico-alumino-phosphate (S-A-P) gels [11, 12]; the structures of these gels are far from fully understood, and the chemical details of the mechanisms involved require further investigation.

The strong monolithic product of the phosphate activation of an aluminosilicate source, such as metakaolin, is sometimes termed a phosphate-based geopolymer [10, 13]. This reaction occurs in an acidic or low-alkaline medium environment in which a phosphate or phosphoric acid solution, rather than the alkali-silicate used in conventional geopolymers, chemically activates the aluminosilicate precursors to yield a compact geopolymer matrix with a condensed structure of silico-alumino-phosphate linkages [14, 15]. It has been claimed that the newly formed Al-O-P linkages could balance the charge caused by changes in the chemical environment of

69 aluminum [16], as is also observed in the synthesis of charge-neutral crystalline zeolite-like

70 aluminophosphate and silico-alumino-phosphate frameworks [17]. Thus, a charge balance

71 within the molecular structure is achieved without the involvement of monovalent cations. The

72 above mechanisms create a silico-aluminophosphate geopolymer with low efflorescence and

73 dielectric loss features, which are difficult to achieve in alkali-aluminosilicate geopolymers [16,

74 18].

75

76 Previous investigations on silico-aluminophosphate geopolymers [22-24] indicated that thermal

77 curing (e.g., under sealed conditions at 60°C or 80°C) was usually needed to achieve fast setting

78 and high early strength. This curing method can be accepted for precast geopolymer products

79 but may impose difficulty in on-site operations, especially for larger-scale engineering

80 applications. Thermal curing also consumes a significant amount of energy. To obtain an

81 ambient-temperature hardening mechanism in alkali-activated geopolymers, soluble silicate is

82 generally introduced in the alkaline activating solution because a high concentration of

83 dissolved silicate can facilitate a rapid sol/gel transition that leads to the development of a

84 compact matrix with useful early strength [25, 26]. The addition of a small dose of $NaAlO_2$ into

85 an alkaline activating solution was also reported to improve the workability of the paste and

86 accelerate the growth of the network structure of the formed geopolymer matrix [27].

87

88 Following these findings for alkaline systems, this study explores the potential to use a

89 corresponding mechanism to improve the early-age characteristics of acidic geopolymers. A

90 second aluminate source, in addition to the aluminosilicate source, is explored in this study as

91 an additive to the phosphate activating solution. It is expected that the aluminum phosphate

92 oligomers which form in a low-pH environment can modify the properties of fresh phosphate-

93 based geopolymer paste and its hardened matrix. Aluminum and phosphorus generally exist in

94 the free state at a pH of less than 3, and form aluminophosphate phases when the pH is increased

95 [28]. Therefore, the addition of soluble aluminum may accelerate geopolymerization in the

96 early stage of reaction to achieve an applicable setting time and early strength. A conceptual

97 scheme for the reaction of an aluminosilicate source activated by alkali and phosphate to

98 synthesize alkali-aluminosilicate and silico-aluminophosphate geopolymers, respectively, is

99 displayed in Fig. 1, which illustrates the activating solution-accelerated formation processes

100 from an aluminosilicate source to a geopolymer.

101

102 In this study, to assess the effectiveness of the addition of soluble aluminum species into a

phosphate activating solution for synthesizing geopolymers, various contents of soluble aluminum source were introduced, with the aim of modifying the setting time and rheological properties of the fresh geopolymer pastes at room temperature. The effects of the soluble aluminum species on the molecular structure of the resulting fresh and hardened geopolymer pastes were elaborated by liquid-state nuclear magnetic resonance (NMR) spectroscopy, other spectroscopic and thermal analyses. Microstructural features of the hardened geopolymer pastes as a function of Al addition were also explored by scanning electron microscopy (SEM) and mercury intrusion porosimetry (MIP).

2. Experimental

2.1 Materials and mix proportions

The phosphate-based geopolymer pastes were formulated to achieve designed molar ratios of silicon, aluminum and phosphorus. Metakaolin (MK) (KAOPOZZ, Chaopai Kaolin Co., Ltd., China) was used as the aluminosilicate source. The composition of MK was detected by X-ray fluorescence, on an ignited mass basis (LOI: 4.1%), as SiO_2 (51.1%), Al_2O_3 (46.8%), TiO_2 (0.8%), Fe_2O_3 (0.5%), CaO (0.2%), SO_3 (0.2%), and others (0.4%). The phosphate activating solution was prepared using orthophosphoric acid H_3PO_4 (OPA, 85 wt.% in H_2O, Ajax Finechem Laboratory Chemicals), liquid monoaluminum phosphate (MAP, $Al(H_2PO_4)_3$, 61.3 wt.% in H_2O, Xianju Litian Chemical Co. Ltd.), and deionized water. Three soluble aluminum contents (i.e., Al/P molar ratios of 0, 0.1, and 0.3) in the activating solutions were designed to represent control, low-content aluminum and high-content aluminum groups. The MAP supplied the soluble aluminum species in the activating solution, and had little influence on the initial pH value (as shown in Table 1). Silico-aluminophosphate geopolymers with a constant H_2O/MK mass ratio of 0.40 and a fixed Si/P molar ratio of 2.75 were produced by mixing the activating solution with the MK particles. As listed in Table 1, six different mix proportions were used, although the mixes A0-0.5, A1-0.5, and A2-0.5 were used only for tests of rheological properties.

OPA, MAP, and deionized water were fully blended in the specified proportions and cooled down to room temperature for use as the activating solutions, which were then mechanically homogenized with the MK particles for 5 min to form fresh geopolymer pastes. Before casting into 40×40×40 mm plastic molds, the respective rheological and flow properties of the fresh

5

geopolymer pastes and their initial and final setting times were measured. The hardened geopolymer pastes were demolded 48 hours after casting, and cured in moist conditions (95% to 100% relative humidity) at room temperature for specified periods.

2.2 Test methods

The characterization of the fresh geopolymer pastes was performed as follows:

(1) A rotational and oscillatory rheometer (Anton Paar MC302) equipped with a parallel-plate measuring system (maximum torque, 200 mN·m) was applied to measure the rheological properties of the fresh geopolymer pastes at a temperature of 25 °C by monitoring the evolution of shear stress (Pa) and viscosity (Pa·s) under shear rates ranging from 0.01 to 100 s^{-1}. The solid volume fractions of the geopolymer pastes with the two H_2O/MK ratios (0.4 and 0.5) were about 0.78 and 0.70, respectively, to ensure that the paste displayed a yield stress [29].

(2) The macroscopic fluidity of the fresh geopolymer pastes was determined by a mini-cone slump flow test setup [30] with an upper diameter of 36 mm, lower diameter of 60 mm, and height of 60 mm.

(3) The initial and final setting times of the geopolymers were determined using a Vicat apparatus according to BS EN 196-3: 2005.

(4) The liquid-state ^{31}P and ^{27}Al NMR spectra for the MAP and activating solutions were obtained using a Bruker 400 spectrometer at ambient temperature. The spectrometer frequencies for ^{31}P and ^{27}Al nuclei were 202.47 and 130.33 MHz, respectively. The corresponding recycle delays applied were 6 and 5 s, with 90º pulse durations of 8 and 2 μs, respectively. The chemical shifts of ^{31}P were expressed in ppm relative to the OPA, and the ^{27}Al resonances were referenced to a 1.0 mol/L $AlCl_3$ solution.

The compressive strength of the hardened geopolymer pastes was assessed before the spectroscopic, thermal, and microstructural analyses:

(1) The compressive strength of the 40-mm geopolymer paste cubes was measured after 3, 7, 14, and 28 days of curing by a mechanical testing instrument (Testometric CXM 500-50 kN) with a loading rate of 0.8 kN/s (about 0.5 MPa/s) following the guidance of ASTM C109/C109M-16a for load application.

(2) The crushed samples were then manually ground for crystalline phase analysis by X-ray diffractometry (XRD, Rigaku SmartLab) with a 9 kW Cu-Kα radiation source (λ=1.5406 Å)

171   and a scanning step of 0.02° (2□□.

172 (3) Simultaneous thermal analysis under an argon atmosphere (Thermo plus EVO2, Rigaku)

173   was performed to analyze the thermal decomposition and phase transition behaviors of the

174   hardened pastes, at a heating rate of 10 ºC min^{-1}.

175 (4) The microstructural features were characterized by SEM (JEOL, JSM-6490) with energy-

176   dispersive X-ray spectroscopy (EDS, Oxford INCA Energy 250). An acceleration voltage

177   of 20 kV was applied. Before the microscopic measurement, the samples were desiccated

178   (60 °C for 24 h) and surface coated with gold sputter.

179 (5) The pore size distribution of the samples was assessed by MIP (Micromeritics AutoPore

180   IV9500). A geometrical model based on the Washburn equation, as shown in Eq. (1), was

181   applied to determine the pore diameter.

$$D = -4\gamma cos\theta \, / \, P \tag{1}$$

183 where, D (m) is the calculated pore diameter, γ (N/m) is the surface tension, θ (°) is the contact

184 angle between mercury and pore wall, and P (Pa) is the applied pressure. The surface tension

185 (γ) and contact angle (θ) selected in this study were 0.485 N/m and 140°, respectively. The

186 applied pressure (P) ranged from 0.007 to 207 M Pa.

187

188 **3. Results and Discussion**

189

190 3.1 Fresh geopolymer pastes

191

192 *3.1.1 Rheology*

193

194 The Bingham model (Eq. (2)) is often used to approximate the rheological behavior of a

195 hydraulic or geopolymer cement paste in terms of the shear stress-shear rate relationship over

196 a specific range [31, 32]:

$$\tau = \tau_0 + \eta_0\gamma \tag{2}$$

198 where τ (Pa) is the shear stress, γ (s^{-1}) is the shear rate, and τ_0 (Pa) and η_0 (Pa·s) are the yield

199 stress and plastic viscosity, respectively.

200

201 In particulate pastes, the viscosity and yield stress are controlled by colloidal interactions due

202 to electrostatic and van der Waals forces between particles (the MK particles in this case),

203 viscous forces in the interstitial liquid between particles (the activating solution in this case),

204   and direct contact forces [29].

205

206   Figure 2 plots the evolution of the rheological characteristics of the fresh geopolymer pastes,

207   measured as a function of shear rate from 0.01 to 100 s^{-1}. The data shows that the Bingham

208   model provides a reasonable – although not perfect – description of the rheological

209   characteristics of these pastes. There is some deviation from Bingham behavior at the very

210   beginning of the test, which may be related to thixotropic behavior as the MK particles are far

211   from spherical and can thus cause complexities in time-dependent as well as shear-dependent

212   rheology. Comparing between the various samples, it is seen that the presence of more Al

213   species can promote a lower yield stress in the fresh phosphate-based geopolymer paste with a

214   H_2O/MK ratio of 0.4 (i.e., A1-0.4 and A2-0.4). The geopolymer paste prepared using the Al-

215   free activating solution at low water content (i.e., A0-0.4) was beyond the measurement range

216   of the rheometer because of its high stickiness. The yield stress of the A1-0.4 and A2-0.4 pastes

217   as estimated using the Bingham model reached 500 ($\pm$150) and 800 ($\pm$200) Pa, respectively,

218   where the quoted error bounds on the yield stress values reflect the uncertainty introduced by

219   the use of different sections of the flow curves to determine the yield stress via Eq. (2). The

220   addition of a higher dose of Al to the activating solution (A2-0.4) gave a lower yield stress, and

221   according to the Bingham model fitting results (i.e., the slope of fitting curves), the geopolymer

222   paste with an Al/P molar ratio of 0.3 has a lower viscosity compared to A1-0.4 geopolymer

223   paste. The Al species in the activating solution acted to some extent as a plasticizer, enabling

224   the geopolymer paste to obtain improved workability, which was favorable for producing a

225   compact and dense matrix with high early strength.

226

227   When the H_2O/MK ratio was increased to 0.5, the three geopolymer pastes all displayed

228   improved workability, with yield stress values of 100 to 200 Pa for all pastes at this water

229   content. Similarly to the H_2O/MK = 0.4 series, the geopolymer paste with the most Al species

230   in its activating solution (A2-0.5) had the lowest yield stress. However, for this set of samples

231   at high water content, the addition of Al to the activator can evidently lower the yield stress of

232   the fresh geopolymer paste while maintaining the viscosity, as seen by the fact that the flow

233   curves for all three -0.5 series samples in Figure 2 are parallel at moderate to high shear rate.

234

235   *3.1.2 Macroscopic fluidity and setting time*

236

237   It is well known that the fluidity of cement paste is mainly influenced by water usage (i.e., the

238 water-to-cement ratio in conventional cements). Figure 3a compares the flows (in terms of the

239 diameter spread on a glass plate in a mini slump test) of the geopolymer pastes with varying

240 aluminum contents, at a fixed H_2O/MK ratio of 0.4. The flow increased significantly with the

241 Al/P ratio in the activating solutions. An Al/P ratio of 0.3 led to an increase of the flow diameter

242 by 50% (106 mm) as compared to the reference case of Al/P=0, whose flow diameter was just

243 78 mm in 60 s. Dividing the flow more specifically into faster and slower processes (i.e.,

244 distinguishing yield stress control from viscous control), the fluidity in the first period between

245 0 and 30 s dominated in the flow test, consistent with the moderate yield stress but relatively

246 low plastic viscosity observed in Figure 2 for each of these pastes. The flow diameter of paste

247 A2 reached about 92 mm, whereas that reached by paste A0 during this period was only 58 mm.

248 However, an opposite trend was observed from 30 to 60 s, whereby the flow diameter for A0

249 further increased by 19 mm and that for A2 increased by 14 mm. These results indicate that the

250 involvement of aluminum species greatly improved the macroscopic fluidity.

251

252 Achieving a reasonable setting time is critical to engineering applications of any cement to be

253 used at ambient temperature. The setting results shown in Fig. 3b demonstrate the difference

254 between the geopolymers with and without the added aluminum species. In the early period,

255 slow dealumination from the MK particles occurred when encountering the activating solution

256 to form an inter-grain gel [32]. The initial setting of the geopolymer pastes stemmed from the

257 free aluminum species combining with phosphate to form an aluminophosphate gel [28].

258 Therefore, the long initial setting time in geopolymer A0 might be a result of the release of

259 aluminum into solution from the solid aluminosilicate source (i.e., the dealumination reaction)

260 delaying its hardening, whereas feeding aluminum directly in the activating solution could

261 provide the necessary aluminum in the early stages of reaction without the need to wait for the

262 solid precursor to dissolve to such an extent. Thus, as shown in the results for mixes A1 and A2

263 (Fig. 3b), the free aluminum species in the activating solution could drive a rapid sol/gel

264 transition due to the supplementation of the free Al in the aqueous phase providing the

265 opportunity for near-immediate gel formation. The initial setting times reached a range suitable

266 for engineering applications, although the initial setting time was still rather long (about 3 h).

267 Nevertheless, the free aluminum species, whether supplied from either the activating solution

268 or the solid aluminosilicate source, controlled the reaction rate and affected the setting time of

269 the geopolymer pastes.

270

271 *3.1.3 Liquid-state ^{31}P and ^{27}Al NMR of phosphate activators*

272

Figures 4a and 4b show the liquid-state ^{31}P and ^{27}Al NMR spectra, respectively, of the MAP solution and the two activating solutions mixed with different Al contents, to further explain the experimental results for the fresh geopolymer pastes. From the ^{31}P spectra for all three solutions (Fig. 4a), three distinct bands at 0 to -1.5 ppm, -8 to -9 ppm, and -12 to -14 ppm were detected, and attributed to Q^0, Q^1 and Q^2 phosphate structural units, respectively [33]. The orthophosphate group (i.e., phosphoric acid molecules and ions [34]) generates the phosphorus environment of Q^0, while the two clear signals resonated between -5 to -24 ppm are due to polyphosphates – either sites with P-O-P linkages (-7~-9 ppm), or Al complexed to phosphate-containing ligands (-12~-14 ppm) [34-36]. The band assigned to P-O-P linkages is caused by the species $[Al(L)]^{m+}$ (where L is H-bonded polymeric OPA, such as $H_6P_2O_8$), while the band centered at a chemical shift of around -13 ppm is associated to the species of $[Al(H_2O)_5(H_2PO_4)]^{2+}$ and trans-$[Al(H_2O)_4(H_2PO_4)_2]^+$ as a result of ionic bonding between Al and P [37]. Since the A1 solution was prepared by using small dosage of the MAP solution to dilute the OPA for a resulting Al/P molar ratio of 0.1, the spectrum of the A1 solution in Fig. 4a is embodied by a sharp resonance peak at -0.5 ppm and two small resonances at -8 and -13 ppm. This indicates that the Q^0 phosphate structural unit is dominated in the A1 activating solution with marginal Q^1 and Q^2 phosphate structural units. Similarly, the A2 activating solution prepared by a higher ratio of MAP/OPA (Al/P molar ratio is 0.3) contains more Q^0 and Q^2 phosphate structural units but little Q^1 phosphate structural unit. The addition of Al to adjust the Al/P ratio did not change the chemical environmental of phosphorus when the molar ratio of aluminum to phosphorus was less than 1.0 [34]. However, an increase in the intensity of the band at -8 ppm with decreasing Al content is observed. The resonances assigned to aluminophosphate oligomers (i.e., -12 ~-14 ppm) are intensified (enriched and broadened) with increasing Al content in phosphate activators, which is the result of chemical exchanges between Al and P. This chemistry can break the long phosphate chains (P-O-P linkages) and decrease the polymerization degree [34, 37]. The oligomers formed as a result of the chain breakage benefit the workability of the geopolymer paste, as measured via yield stress and viscosity (in Fig. 2) and fluidity (in Fig. 3.1a).

301

The resonances that are evident in the ^{27}Al spectra at around -8 ppm, and between 80 to 65 ppm, were due to the aluminum species in MAP, in which a clear hexa-coordinated environment of aluminum (i.e., -1 to -9 ppm) was identified (Fig. 4b) [34, 38]. It has previously been reported that the hexa-coordinated aluminum species is the main form of Al in a hardened phosphate-

10

306   activated geopolymer [39]. This is consistent with the addition of Al to the activating solution

307   accelerating the early stage of the geopolymerization process (formation of aluminate and

308   phosphate oligomers) under an acidic phosphate environment, thus leading to a shortened

309   setting time. A weak, broad resonance at 80 to 65 ppm can be attributed to a small quantity of

310   tetrahedral aluminum present under these conditions [40]. These results indicated that in this

311   pH range (i.e., below 2.0, see Table 1) the OPA did not change the hexa-coordinated Al

312   environment seeded by the MAP. However, as observed in the ^{31}P NMR spectra, the intensity

313   and breadth of the bands resonating at 0 to -20 ppm increase with Al contents in the phosphate

314   activators, which can be attributed to the chemical bonding between Al and P species to form

315   low polymeric units [37].

316

317   3.2 Hardened geopolymer paste

318

319   *3.2.1 Compressive strength*

320

321   As displayed in Fig. 5, the hardened geopolymer pastes prepared with varying Al/P ratios

322   showed significant differences in strength development from 3 to 28 d. In the early stage at 3

323   and 7 d, the existence of soluble aluminum species in the activating solution caused significant

324   enhancement of the compressive strength. Compared with mix A0 (Al/P=0), mix A2 (Al/P=0.3)

325   showed strengths that were higher by 14.1 MPa and 15.1 MPa at 3 and 7 d, respectively.

326   Geopolymer A2 remained almost the same strength from 7 d up to 28 d. In comparison, the

327   most significant increase in the compressive strength was achieved in geopolymer A0 (with no

328   aluminum species in the activating solution), which evolved from 22.1 MPa at 7 d to 51.3 MPa

329   at 28 d. The strength of the geopolymer A1 (Al/P=0.1) was moderately improved at both 3 and

330   7 d, but the strength growth thereafter was inferior to that of geopolymer A0. It seems that the

331   hardening during the early period caused by the addition of free aluminum species in the

332   activating solution can compromise or hinder the ongoing reaction of MK (involving

333   dealumination and delamination to provide nutrients for gel growth) in the latter period.

334   Therefore, a tradeoff was found between the early-state strength and the long-term strength,

335   depending on the content of Al in the activating solution.

336

337   *3.2.2 X-ray diffraction*

338

339   The XRD patterns of the 28 d hardened geopolymers shown in Fig. 6 indicate that no new

340   crystalline phase was generated in this reaction process. The only distinct peak in any of the

341   diffractograms is assigned to the quartz that was already present in the unreacted MK particles.

342   The geopolymerization of aluminosilicates, regardless of the activation approach (either by

343   alkali or phosphate activation), involves the dissolution and reconstruction of aluminates and

344   silicates to form disordered gels [41, 42]. In Fig. 6a, a visible difference between the

345   geopolymers and the MK is the change in the broad diffuse peak at 15º to 30º (2θ), whose

346   enlarged view is shown in Fig. 6b. It can be seen that the diffuse peak partially disappears and

347   shifts after the reaction, especially for geopolymer A0. For geopolymers A1 and A2, the diffuse

348   peak is weakened and shows much less intensity in the range 22º to 26º (2θ) compared with that

349   of the MK particles. Similar findings were reported by Cui et al. [16], Douiri et al. [42], and

350   Louati et al. [12], although they all used H_3PO_4 without additional Al to activate the

351   aluminosilicate precursors for synthesis of silico-aluminophosphate geopolymers. These

352   spectral changes can be attributed to the effect of phosphate activation on the MK particles.

353   Considering the XRD pattern of MK as a reference, a larger diffuse peak change (at 18 to 28º)

354   in geopolymer A0 than that in the other geopolymers indicates that the degree of reaction of the

355   MK particles in geopolymer A0 was higher than that of the others at 28 d, consistent with the

356   compressive strength data and confirming that the addition of free aluminum species into

357   geopolymers A1 and A2 may, to some extent, hinder the ongoing reaction of MK in the latter

358   period of curing.

359

360   *3.2.3 Thermogravimetry*

361

362   The thermogravimetric/differential thermal analysis (TG-DTA) thermograms for the hardened

363   geopolymer pastes, normalized to the basis of constant mass of MK, are shown in Fig. 7. For

364   all geopolymers, four distinct groups of decomposition or phase transition peaks are observed

365   in the DTA curve: one is located between 100 and 150 ºC, and the others are located in the

366   ranges of 160 to 230 ºC, 800 to 840 ºC, and 980 to 1010 ºC.

367

368   The weight loss at 100 to 150 ºC, accompanied by a sharp endothermic peak in the DTA curves,

369   is attributed to the removal of physically adsorbed water and the dehydration of some of the

370   water-containing gels (loss of loosely chemically bonded water), which accounted for more

371   than 80% of the total weight loss. The subsequent weight loss from 150 to 1050 ºC is marginal

372   in each geopolymer, and largely parallels the TGA curve of the MK; this is attributed mainly to

373   dehydration and dehydroxylation of remnant MK particles within the hardened binder, with a

374 potential minor contribution from any remaining chemically bound water in the reaction
375 product gels.

376

377 The features at 160 to 230 ℃ and 800 to 870 ℃, respectively, show exotherms in the DTA data
378 but no notable corresponding mass loss, and so are likely to relate to phase transitions in the
379 newly formed binder gel. These may be assigned to the amorphous aluminum phosphate phase
380 transforming into trigonal (α-AlPO$_4$) and tetragonal (β-AlPO$_4$) berlinite at elevated temperature
381 [43], which is an exothermic process. These two peaks were not detected in the MK particles.
382 The last phase transition was the formation of mullite from residual, fully dehydroxylated MK
383 particles at 980 to 1010 ℃ [44], and is especially prominent in the raw MK particles. For all
384 geopolymer samples, such a peak is less significant, indicating that the raw MK particles had
385 reacted with the phosphate activating solution to synthesize new gels: silico-alumino-phosphate
386 (S-A-P) gel [16] and amorphous or semi-crystalline aluminum phosphate compounds [12, 17].
387 The presence of similar peaks representing thermally induced processes in all of the
388 geopolymers reveals that there were similar reaction products regardless of the Al/P ratio of the
389 activating solutions. In other words, the compositions of the resulting gels were not strongly
390 influenced by changes in the activating solution with different Al/P ratios.

391

392 *3.2.4 Microstructure*

393

394 However, the pore structures of the geopolymer products did exhibit notable differences when
395 the level of soluble aluminum species was varied (Fig. 8). The MIP results indicate that the
396 porosity of the geopolymer pastes cured for 28 d increased with the Al/P ratio of the activating
397 solutions used, from 17.1% in geopolymer A0 to 18.9% in geopolymer A1 and 21.5% in
398 geopolymer A2 (Fig. 8a). This porosity result is in agreement with the trend in their strength
399 behaviors (i.e., a higher-strength matrix showed lower porosity). The pore diameters accessible
400 to mercury were mainly concentrated between 5 and 1000 nm (Fig. 8b), and can be divided into
401 gel pores (less than 10 nm), small capillary pores (10 to 50 nm), medium capillary pores (50 to
402 100 nm) and large capillary pores (100 to 10 μm) [45-47]. Fig. 8c shows the differential pore
403 diameter distributions and the diameter range between 10 and 1000 nm is enlarged in Fig. 8d.
404 It can be seen for all geopolymers that the capillary pores (small, medium, and large)
405 contributed more than 90% of the porosity. However, the incorporation of aluminum species in
406 the activating solution changed the distribution characteristics of the capillary pores. An
407 increase in the Al content of the activating solution led to a shift to larger capillary pores. The

13

408 pore size distribution of the geopolymer with the most soluble aluminum (i.e., A2 with an Al/P

409 ratio of 0.3) exhibited a sharp maximum at around 90 nm. The other geopolymer samples (A0

410 and A1) showed similar differential porosity distributions to each other, with peak values at 60

411 nm and 73 nm, respectively. These different distributions of the capillary pores will eventually

412 govern the strength and transport properties of the geopolymer matrix. A delayed or

413 compromised dealumination reaction of the metakaolin particles is more likely to produce

414 discontinuous gels that generate inter-gel spaces which form medium and large capillary pores.

415

416 The features identified through this analysis of pore structure are supported by the morphologies

417 and elemental analysis obtained by SEM and EDS. Fig. 9 shows SEM results for the hardened

418 geopolymer pastes cured at 3 d. As shown in Fig. 9a, the A0 matrix consisted of many isolated

419 particles intermixed with gel-like lumps. In the image with higher magnification (Fig. 9b), some

420 discontinuous phases and micro cracks are found, implying a weak reaction between MK and

421 Al-free activators at the early period. The EDS analysis (Fig. 10) indicates the presence of

422 different Al:Si:P ratios at different locations. For instance, points 1 and 2 corresponded to the

423 unreacted MK particles (aluminosilicates without P) and the newly-formed S-A-P gels (reaction

424 products), respectively. As a comparison, the presence of soluble aluminum species in the

425 phosphate activator led to a more compact matrix after the 3 d curing process (in Fig. 9c),

426 although such curing was insufficient for geopolymerization between the MK particles and the

427 activating solution. The enlarged image of the A2 geopolymer cured at 3 d (Fig. 9d) shows a

428 high-continuity texture without isolated phases and micro cracks. The EDS analysis for the

429 compact area (i.e., area 1 in Fig. 9c and Fig. 10) reveals the presence of Si, Al and P, which is

430 very likely to be the result of S-A-P gel formation. However, compared to the EDS spectrum of

431 Point 2, a lower silicon content in this gel indicates that the presence of soluble Al and P species

432 may form aluminophosphate gels for early strength improvement (Fig. 5).

433

434

435 The morphologies of the three geopolymer samples imaged at 28 d revealed that the use of

436 excessive aluminum species (A2, shown in Fig. 11c) was unfavorable due to the production of

437 discontinuous gels as compared with A0 (Fig. 11a). Geopolymer A1 with a moderate content

438 of soluble aluminum species (Fig. 11b) seemed to present an intermediate state between A0 and

439 A2. These microstructural observations coincided well with the strength variation and

440 development of the three geopolymer matrices as discussed above, where the longer-term

441 strength evolution of A2 beyond 7 days was negligible while A0 continued to gain more strength.

14

4. Conclusions

The effects of the addition of soluble aluminum species into a phosphate activating solution for geopolymer synthesis on fresh and hardened properties were investigated in terms of workability, compressive strength, and the microstructure.

The incorporation of aluminum species into the phosphate activating solution allowed a rapid sol/gel transition in the early state due to the supplementation of the free Al (in six-coordination). As a result, the fresh geopolymer paste achieved good workability. The role of aluminum species was similar to that of a plasticizer, lowering the yield stress of the fresh geopolymer paste while keeping the viscosity unchanged. As a result, a compact and dense matrix was obtained with a high early strength of up to 37 MPa at 7 d of curing.

However, the use of soluble aluminum species may also lead to relatively poor strength development in the latter stage depending on the added dose. A geopolymer with an excessive amount of aluminum species may exhibit significant inter-gel spaces (medium capillary pores) due to the formation of discontinuous gels and inability to close and refine these pores at later age, because the accelerated hardening and gel formation blocks the unreacted MK particles and hinders their dealumination reaction.

References

[1] Davidovits, J. (1991). Geopolymers: Inorganic polymeric new materials. *Journal of Thermal Analysis*, **37**: 1633-1656.

[2] Ismail, I., Bernal, S. A., Provis, J. L., San Nicolas, R., Hamdan, S., & van Deventer, J. S. J.

476   (2014). Modification of phase evolution in alkali-activated blast furnace slag by the
477   incorporation of fly ash. *Cement and Concrete Composites*, **45**, 125-135.

478 [3] Juenger, M. C. G., Winnefeld, F., Provis, J. L., & Ideker, J. H. (2011). Advances in
479   alternative cementitious binders. *Cement and Concrete Research*, **41**(12), 1232-1243.

480 [4] Provis, J. L., Palomo, A., & Shi, C. (2015). Advances in understanding alkali-activated
481   materials. *Cement and Concrete Research*, **78**, 110-125.

482 [5] Ouellet-Plamondon, C., & Habert, G. (2015). Life cycle assessment (LCA) of alkali-
483   activated cements and concretes. In *Handbook of alkali-activated cements, mortars and*
484   *concretes*, pp. 663-686.

485 [6] Ding, Y., Dai, J. G., & Shi, C. J. (2016). Mechanical properties of alkali-activated concrete:
486   a state-of-the-art review. *Construction and Building Materials*, **127**, 68-79.

487 [7] Provis, J. L. & van Deventer, J. S. J. (2014). *Alkali-activated materials: state-of-the-art*
488   *report, RILEM TC 224-AAM*. RILEM/Springer, Dordrecht.

489 [8] Provis, J. L. & Bernal, S. A. (2014). Geopolymers and related alkali-activated materials.
490   *Annual Review of Materials Research,* **44**(1), 299-327.

491 [9] Wagh, A. S. (2005). Chemically bonded phosphate ceramics—a novel class of
492   geopolymers. *Ceramic Transactions*, **165**, 107-116.

493 [10] Davidovits, J. (2011). *Geopolymer: chemistry & applications, 3rd edition*. Geopolymer
494   Institute, Saint-Quentin.

495 [11] Louati, S., Baklouti, S., & Samet, B. (2016). Acid based geopolymerization kinetics: Effect
496   of clay particle size. *Applied Clay Science*, **132**, 571-578.

497 [12] Louati, S., Hajjaji, W., Baklouti, S., & Samet, B. (2014). Structure and properties of new
498   eco-material obtained by phosphoric acid attack of natural Tunisian clay. *Applied Clay*
499   *Science*, **101**, 60-67.

500 [13] Wang, Y. S., Dai, J. G., Ding, Z. & Xu, W. T. (2017). Phosphate-based geopolymer:
501   Formation mechanism and thermal stability. *Materials Letters*, **190**, 209-212.

502 [14] Cao, D., Su, D., Lu, B., & Yang, Y. (2005). Synthesis and structure characterization of
503   geopolymeric material based on metakaolinite and phosphoric acid. *Journal of the Chinese*
504   *Ceramic Society*, **33**: 1385-1389.

505 [15] Liu, L. P., Cui, X. M., Qiu, S. H., Yu, J. L. & Zhang, L. (2010). Preparation of phosphoric
506   acid-based porous geopolymers. *Applied Clay Science*, **50**: 600-603.

507 [16] Cui, X. M., Liu, L. P., He, Y., Chen, J. Y., & Zhou, J. (2011). A novel aluminosilicate
508   geopolymer material with low dielectric loss. *Materials Chemistry and Physics*, **130**(1-2),
509   1-4.

[17] Derouane, E.G., Fripiat, J.G. and von Ballmoos, R. (1990). Quantum mechanical calculations on molecular sieves. 2. Model cluster investigation of silicoaluminophosphates. *Journal of Physical Chemistry,* **94**(4): 1687-1692.

[18] Zhang, Z., Provis, J. L., Reid, A., & Wang, H. (2014). Fly ash-based geopolymers: the relationship between composition, pore structure and efflorescence. *Cement and Concrete Research*, **64**, 30-41.

[19] Kovalchuk, G., Fernández-Jiménez, A., & Palomo, A. (2007). Alkali-activated fly ash: effect of thermal curing conditions on mechanical and microstructural development–Part II. *Fuel*, **86**(3), 315-322.

[20] Marjanović, N., Komljenović, M., Baščarević, Z., Nikolić, V., & Petrović, R. (2015). Physical–mechanical and microstructural properties of alkali-activated fly ash–blast furnace slag blends. *Ceramics International*, **41**(1), 1421-1435.

[21] Bernal, S. A., San Nicolas, R., Van Deventer, J. S. J., & Provis, J. L. (2016). Alkali-activated slag cements produced with a blended sodium carbonate/sodium silicate activator. *Advances in Cement Research*, **28**(4), 262-273.

[22] Gualtieri, M. L., Romagnoli, M., Pollastri, S., & Gualtieri, A. F. (2015). Inorganic polymers from laterite using activation with phosphoric acid and alkaline sodium silicate solution: mechanical and microstructural properties. *Cement and Concrete Research*, **67**, 259-270.

[23] Douiri, H., Kaddoussi, I., Baklouti, S., Arous, M., & Fakhfakh, Z. (2016). Water molecular dynamics of metakaolin and phosphoric acid-based geopolymers investigated by impedance spectroscopy and DSC/TGA. *Journal of Non-Crystalline Solids*, **445**, 95-101.

[24] He, Y., Liu, L., He, L., & Cui, X. (2016). Characterization of chemosynthetic H_3PO_4–Al_2O_3–$2SiO_2$ geopolymers. *Ceramics International*, **42**(9), 10908-10912.

[25] Duxson, P., Provis, J. L., Lukey, G. C., Mallicoat, S. W., Kriven, W. M., & Van Deventer, J. S. J. (2005). Understanding the relationship between geopolymer composition, microstructure and mechanical properties. *Colloids and Surfaces A: Physicochemical and Engineering Aspects*, **269**(1-3), 47-58.

[26] Jansson, H., Bernin, D., & Ramser, K. (2015). Silicate species of water glass and insights for alkali-activated green cement. *AIP Advances*, **5**(6), 067167.

[27] Benavent, V., Steins, P., Sobrados, I., Sanz, J., Lambertin, D., Frizon, F., Rossignol, S., & Poulesquen, A. (2016). Impact of aluminum on the structure of geopolymers from the early stages to consolidated material. *Cement and Concrete Research*, **90**, 27-35.

[28] Petzet, S., Peplinski, B., Bodkhe, S. Y., & Cornel, P. (2011). Recovery of phosphorus and aluminium from sewage sludge ash by a new wet chemical elution process (SESAL-Phos-

544   recovery process). *Water Science and Technology*, **64**(3), 693-699.

545   [29] Roussel, N., Lemaître, A., Flatt, R. J., & Coussot, P. (2010). Steady state flow of cement

546   suspensions: a micromechanical state of the art. *Cement and Concrete Research*, **40**(1), 77-

547   84.

548   [30] Dai, J. G., Munir, S., & Ding, Z. (2013). Comparative study of different cement-based

549   inorganic pastes towards the development of FRIP strengthening technology. *Journal of*

550   *Composites for Construction*, **18**(3), A4013011.

551   [31] Favier, A., Hot, J., Habert, G., Roussel, N., & d'Espinose de Lacaillerie, J. B. (2014). Flow

552   properties of MK-based geopolymer pastes. A comparative study with standard Portland

553   cement pastes. *Soft Matter*, **10**(8), 1134-1141.

554   [32] Favier, A., Habert, G., d'Espinose de Lacaillerie, J. D., & Roussel, N. (2013). Mechanical

555   properties and compositional heterogeneities of fresh geopolymer pastes. *Cement and*

556   *Concrete Research*, **48**, 9-16.

557   [33] Chavda, M. A., Bernal, S. A., Apperley, D. C., Kinoshita, H., & Provis, J. L. (2015).

558   Identification of the hydrate gel phases present in phosphate-modified calcium aluminate

559   binders. *Cement and Concrete Research*, **70**, 21-28.

560   [34] Samadi-Maybodi, A., Nejad-Darzi, S. K. H., & Bijanzadeh, H. (2009). ^{31}P and ^{27}Al NMR

561   studies of aqueous (2-hydroxyethyl) trimethylammonium solutions containing aluminum

562   and phosphorus. *Spectrochimica Acta Part A: Molecular and Biomolecular Spectroscopy*,

563   **72**(2), 382-389.

564   [35] Abdi, D., Cade-Menun, B. J., Ziadi, N., & Parent, L. É. (2014). Long-term impact of tillage

565   practices and phosphorus fertilization on soil phosphorus forms as determined by [31]P

566   nuclear magnetic resonance spectroscopy. *Journal of Environmental Quality*, **43**(4), 1431-

567   1441.

568   [36] Liu, J., Yang, J., Liang, X., Zhao, Y., Cade-Menun, B. J., & Hu, Y. (2014). Molecular

569   speciation of phosphorus present in readily dispersible colloids from agricultural soils. *Soil*

570   *Science Society of America Journal*, **78**(1), 47-53.

571   [37] Mortlock, R. F., Bell, A. T., & Radke, C. J. (1993). Phosphorus-31 and aluminum-27 NMR

572   investigations of highly acidic, aqueous solutions containing aluminum and phosphorus.

573   *Journal of Physical Chemistry*, **97**(3), 767-774.

574   [38] Haouas, M., Taulelle, F., & Martineau, C. (2016). Recent advances in application of [27]Al

575   NMR spectroscopy to materials science. *Progress in Nuclear Magnetic Resonance*

576   *Spectroscopy*, **94**, 11-36.

577   [39] Perera, D. S., Hanna, J. V., Davis, J., Blackford, M. G., Latella, B. A., Sasaki, Y., & Vance,

578   E. R. (2008). Relative strengths of phosphoric acid-reacted and alkali-reacted metakaolin
579   materials. *Journal of Materials Science*, **43**(19), 6562-6566.

580 [40] Mueller, D., Hoebbel, D., & Gessner, W. (1981). ^{27}Al NMR studies of aluminosilicate
581   solutions. Influences of the second coordination sphere on the shielding of aluminium.
582   *Chemical Physics Letters*, **84**(1), 25-29.

583 [41] Provis, J. L., Lukey, G. C., & van Deventer, J. S. J. (2005). Do geopolymers actually contain
584   nanocrystalline zeolites? A reexamination of existing results. *Chemistry of Materials*,
585   **17**(12), 3075-3085.

586 [42] Douiri, H., Louati, S., Baklouti, S., Arous, M., & Fakhfakh, Z. (2014). Structural, thermal
587   and dielectric properties of phosphoric acid-based geopolymers with different amounts of
588   H_3PO_4. *Materials Letters*, **116**, 9-12.

589 [43] Prado-Herrero, P., Garcia-Guinea, J., Crespo-Feo, E., & Correcher, V. (2010). Temperature-
590   induced transformation of metavariscite to berlinite. *Phase Transitions*, **83**(6), 440-449.

591 [44] White, C. E., Provis, J. L., Proffen, T., Riley, D. P., & van Deventer, J. S. J. (2010). Density
592   functional modeling of the local structure of kaolinite subjected to thermal dehydroxylation.
593   *Journal of Physical Chemistry A*, **114**(14), 4988-4996.

594 [45] Zeng, Q., Li, K., Fen-Chong, T., & Dangla, P. (2012). Pore structure characterization of
595   cement pastes blended with high-volume fly-ash. *Cement and Concrete Research*, **42**(1),
596   194-204.

597 [46] Ma, H., Hou, D., & Li, Z. (2015). Two-scale modeling of transport properties of cement
598   paste: Formation factor, electrical conductivity and chloride diffusivity. *Computational*
599   *Materials Science*, **110**, 270-280.

600 [47] Wang, Y. S., & Dai, J. G. (2017). X-ray computed tomography for pore-related
601   characterization and simulation of cement mortar matrix. *NDT & E International*, **86**, 28-
602   35.

603

Tables and Figures

Table 1. Mix proportions of activating solution and phosphate-based geopolymer.

No.	Raw materials by weight ratio					Fresh geopolymer paste	
	Aluminosilicate source	Activating solution					
	MK[a]	OPA[a]	MAP[b]	Water	Initial pH	Soluble Al species (Al/P)	Si/P molar ratio
A0	10	3.60	0	3.46	1.62	0	2.75
A1	10	2.51	1.98	2.86	1.64	0.1	2.75
A2	10	0.36	5.94	1.65	1.69	0.3	2.75
A0-0.5[c]	10	3.60	0	4.46	1.63	0	2.75
A1-0.5[c]	10	2.51	1.98	3.86	1.66	0.1	2.75
A2-0.5[c]	10	0.36	5.94	2.65	1.69	0.3	2.75

[a] Mass fractions of MK and OPA are 97.9% ($SiO_2 + Al_2O_3$) and 85%, respectively.

[b] Mass concentration of MAP is 61.3% with a P/Al molar ratio of 2.99.

[c] These mixing proportions were provided only for tests of rheological properties. A0-0.5 means the geopolymer A0 is prepared with a H_2O/MK mass ratio of 0.5. A1-0.5 and A2-0.5 are similarly defined.
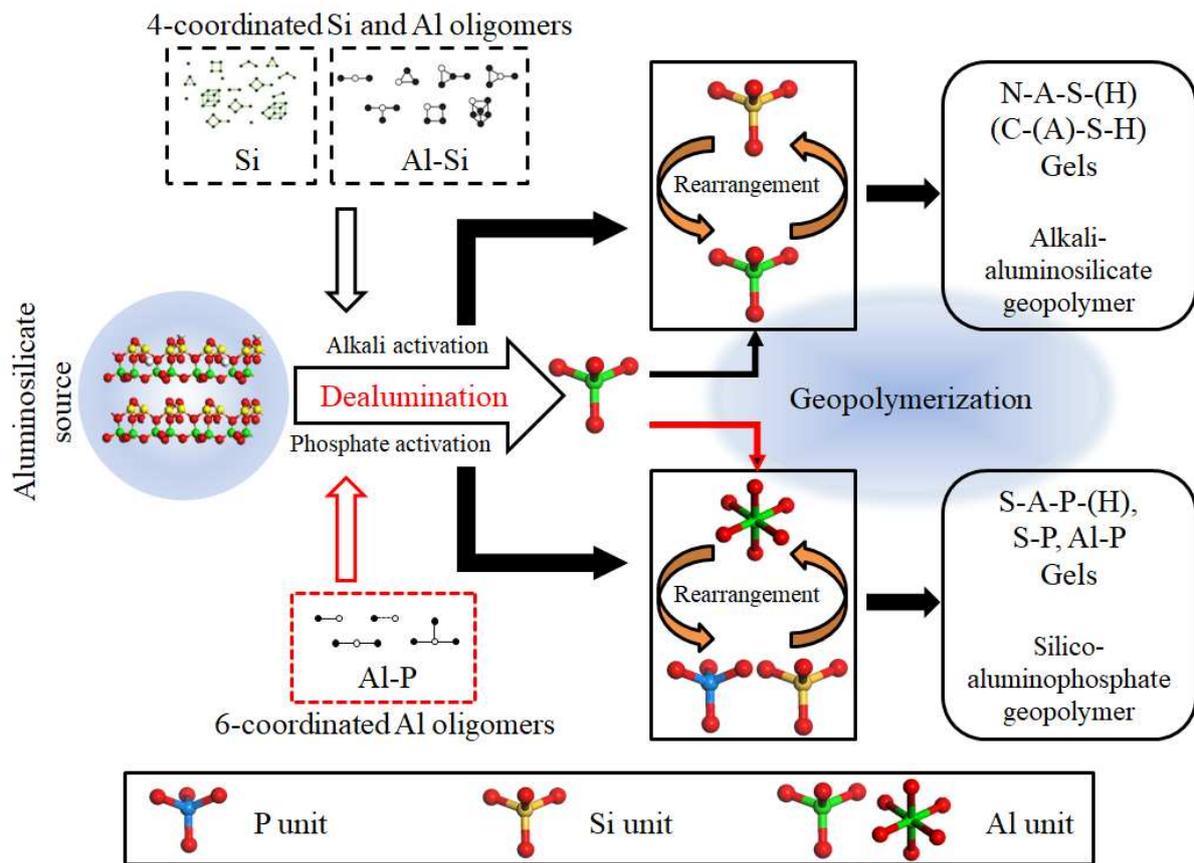
609

610 Fig. 1 Conceptual scheme for an activating solution-accelerated formation process from an

611 aluminosilicate source to a geopolymer. The aluminosilicate source catalyzed by alkali and

612 phosphate synthesizes the respective alkali-aluminosilicate and silico-aluminophosphate

613 geopolymers.

614
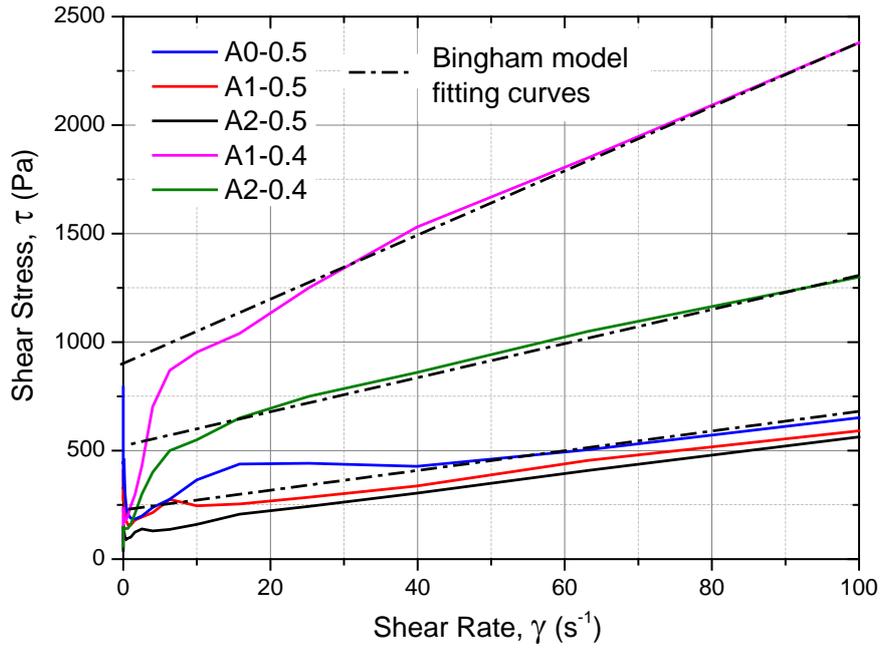
615

616 Fig. 2 Rheological flow curves of the fresh geopolymer pastes with different contents of soluble

617 Al species in their respective activators. The suffix -0.4 or -0.5 in the sample ID indicates the

618 H_2O/MK ratio (0.4 or 0.5). The geopolymer paste prepared using the Al-free activating solution

619 at low water content (i.e., A0-0.4) was outside the measurement range of the rheometer.

620

621

622

(a)

623

624

(b)
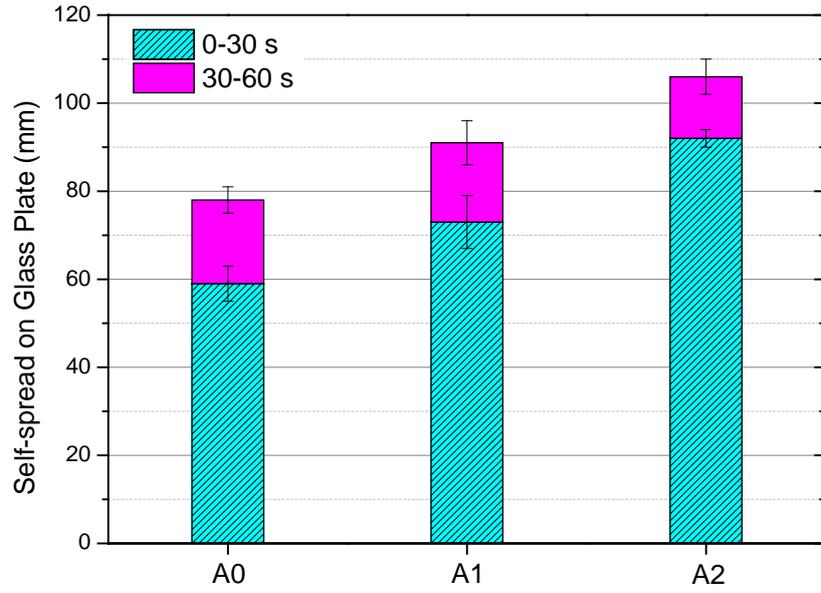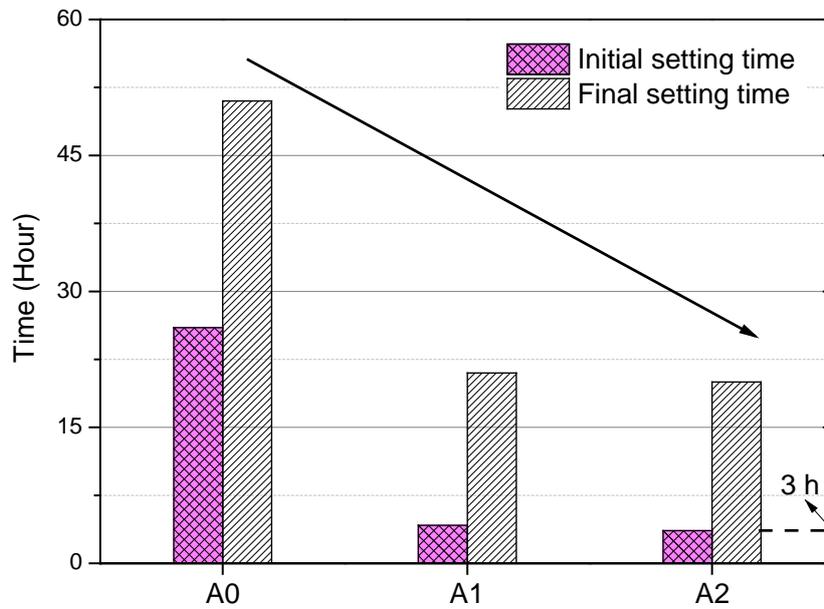
Fig. 3 Fluidity and setting times of the phosphate-based geopolymer pastes with different contents of soluble Al species. (a) Fluidity. (b) Initial and final setting times.

627

628
629

(a)

630
631

(b)
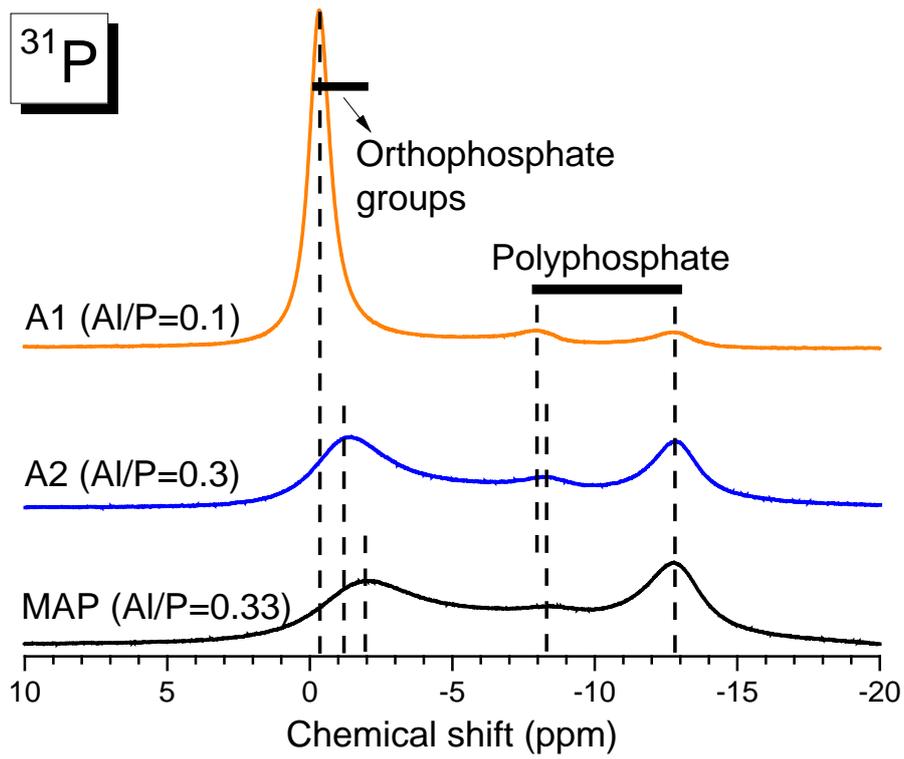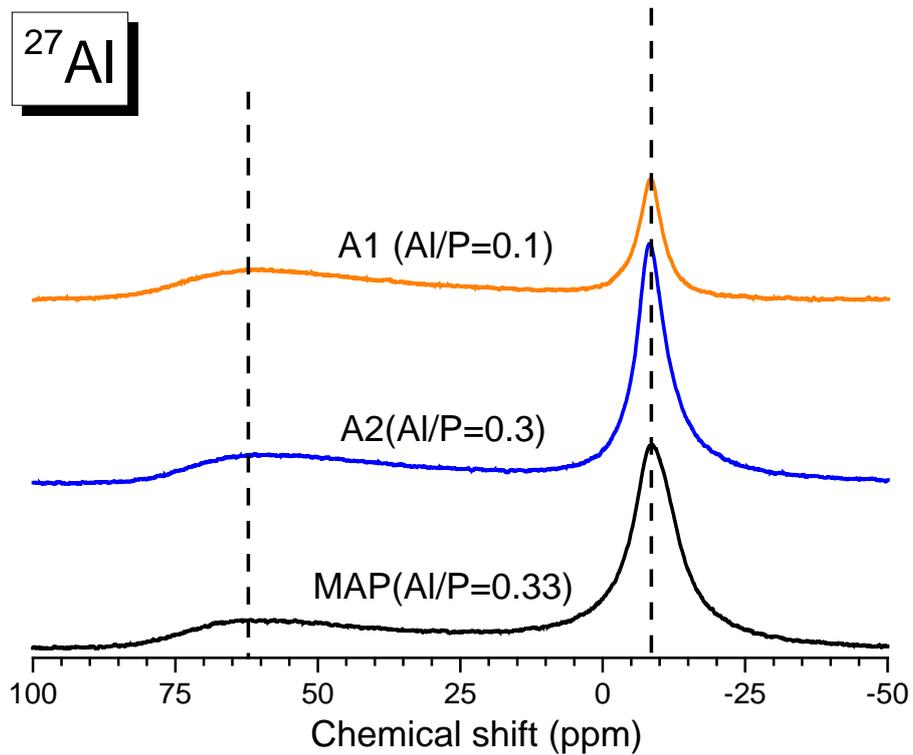
632   Fig. 4 Liquid-state ^{31}P and ^{27}Al NMR spectra for the MAP and activating solutions
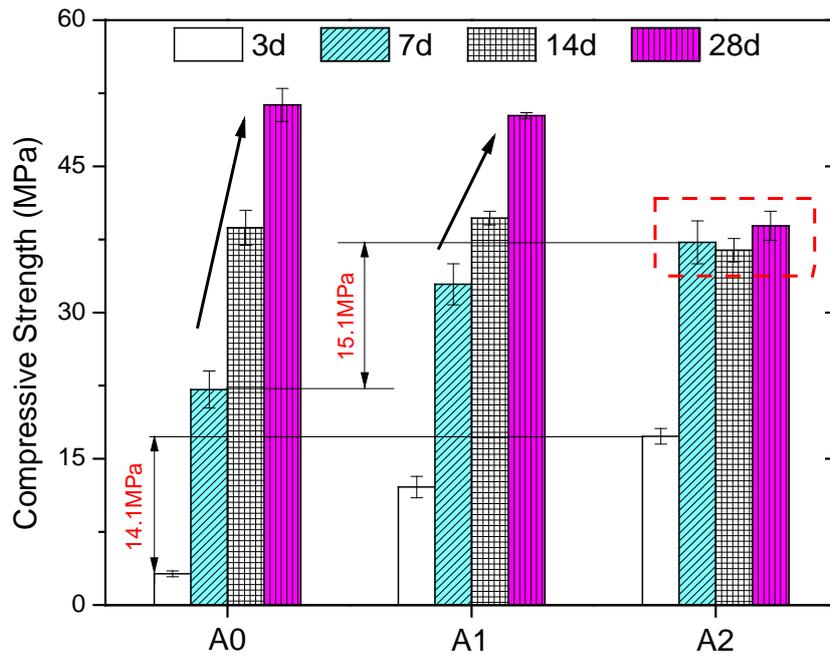
Fig. 5 Compressive strength development for the first 28 days, of the hardened geopolymer pastes with varying contents of soluble Al species.
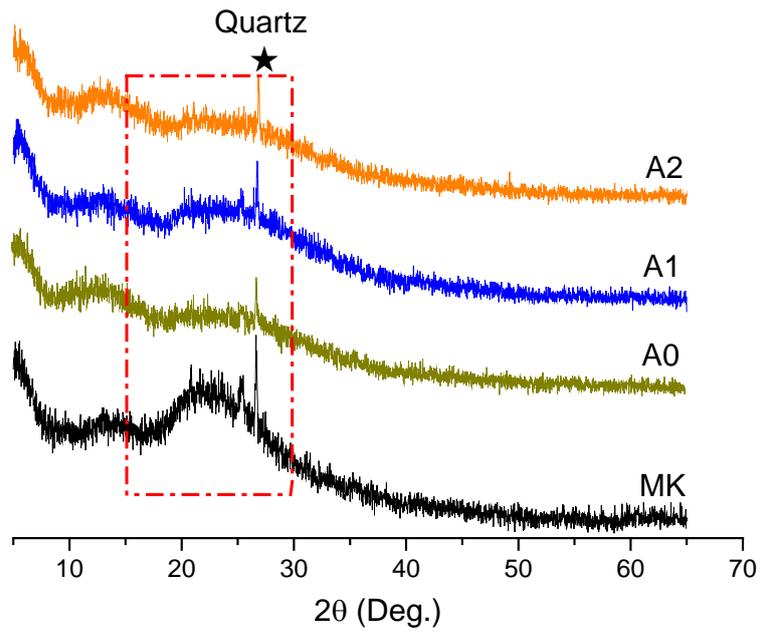
637
638

(a)
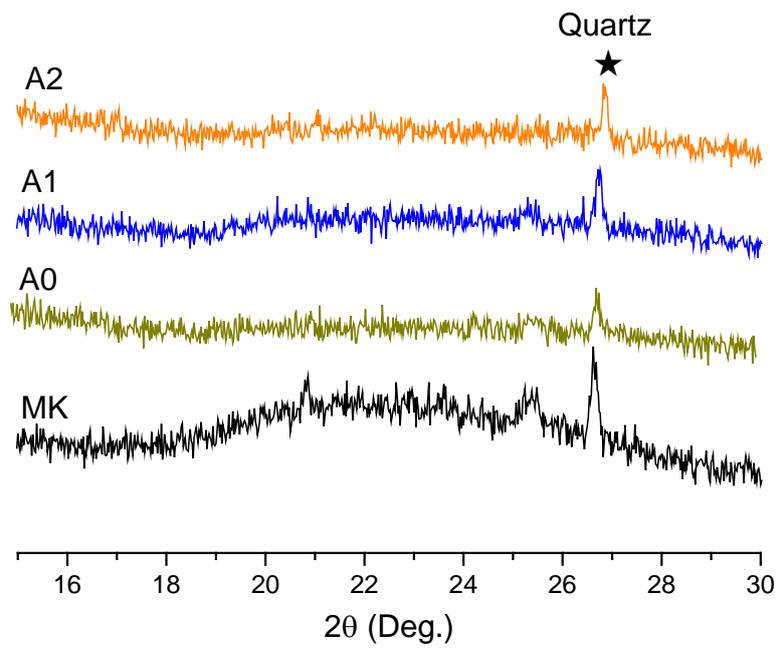
639
640

(b)

641   Fig. 6 XRD patterns of the 28 d cured geopolymers prepared with three different Al/P molar

642   ratios in the activating solution, and the MK precursor. (a) 5º to 65º 2θ; (b) enlarged at 15º to

643   30º 2θ.

644
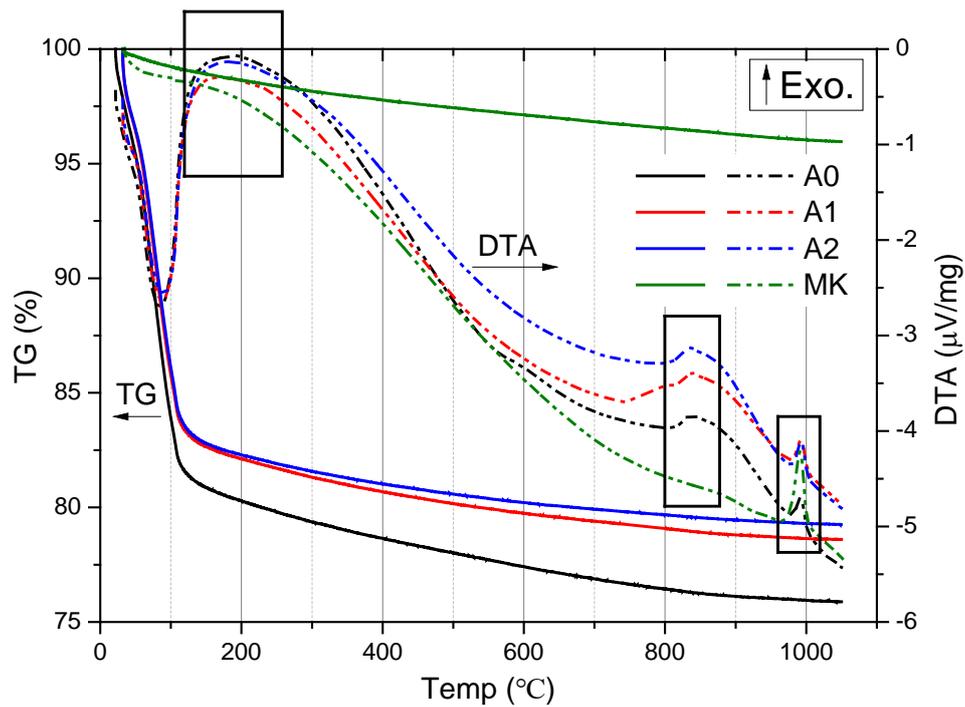
Fig. 7 TG-DTA thermograms for the 28 d cured geopolymers with varying Al/P molar ratios and H_2O/MK ratios.
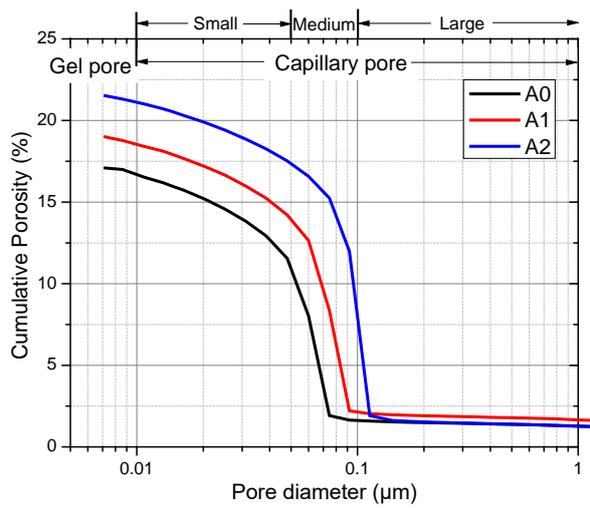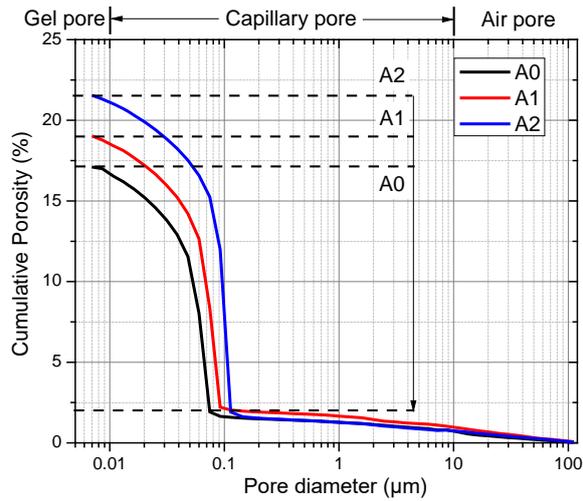
649
650   (a)   (b)
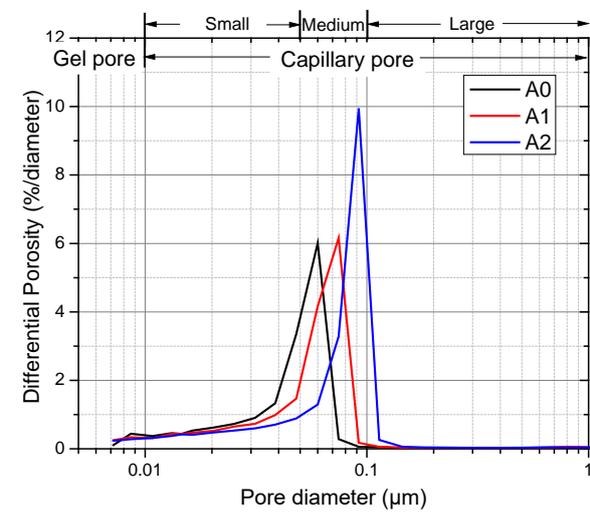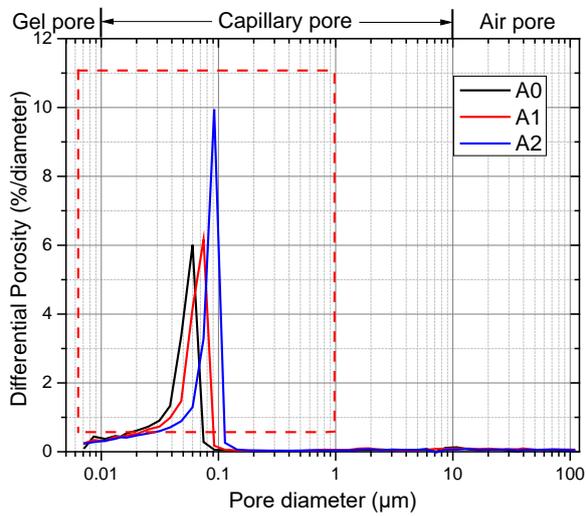
651
652   (c)   (d)

653   Fig. 8 Pore diameter distributions determined by MIP analysis of the three hardened
654   geopolymer pastes at 28 d. (a, b) Cumulative distribution; (c, d) differential distribution.

655

656

657

658
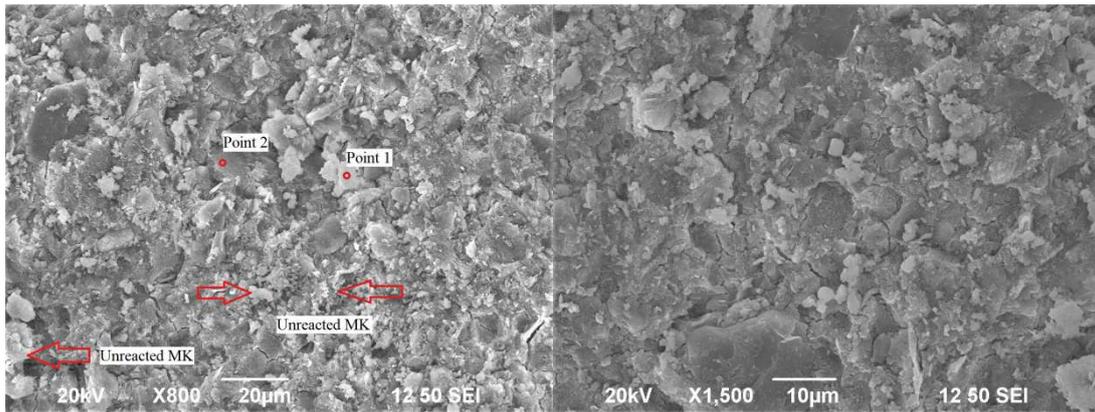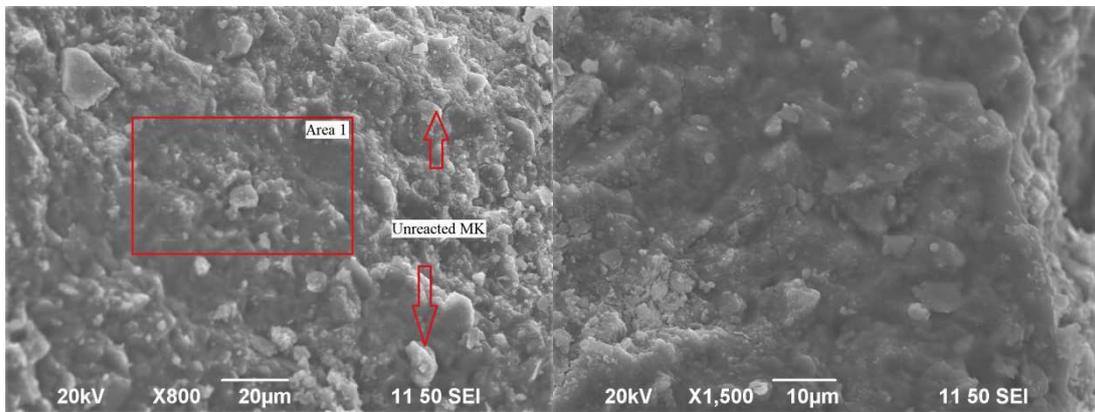
659

660 (c) x800   (d) x1500

661 Fig. 9 SEM results of the hardened geopolymer pastes cured at 3 d. (a) and (b) A0

662 geopolymer; (c) and (d) A2 geopolymer.

663
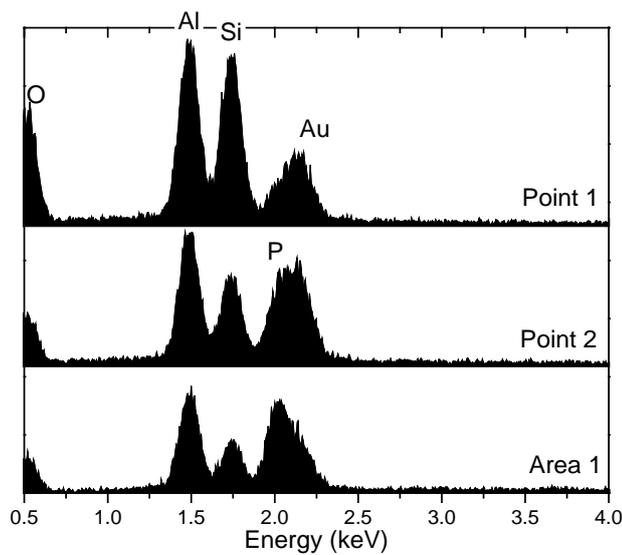
664

665 Fig. 10 EDS results of the hardened geopolymer pastes at 3 d. The point 1 point 2 and area 1

666 can be found in Figs. 9a and 9b.

667
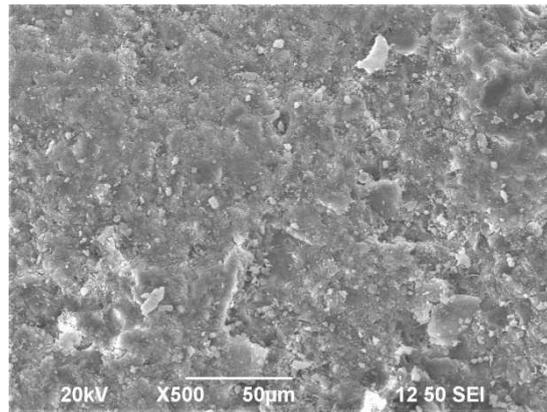
668

669 (a)

670
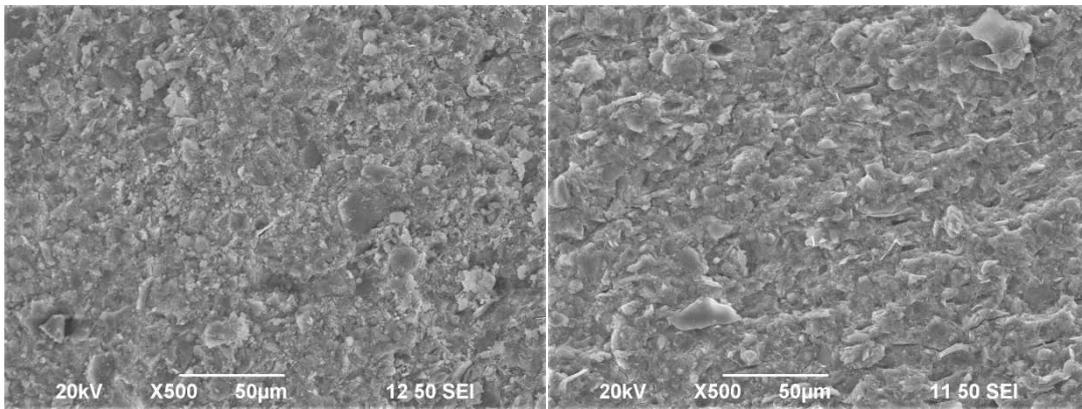
671 (b) (c)

672 Fig. 11 SEM results of the hardened geopolymer pastes cured at 28 d. (a) A0 geopolymer; (b)

673 A1 geopolymer; and (c) A2 geopolymer.